Structural Engineering and Mechanics, *Vol. 67, No. 6 (2018) 659-669*
DOI: https://doi.org/10.12989/sem.2018.67.6.659

Dynamic analysis of non-symmetric FG cylindrical shell under shock loading by using MLPG method

Yaser Sadeghi Ferezghi[1a], Mohamad R. Sohrabi[1b] and Seyed M. MosaviNezhad[*2]

[1]*Department of Civil Engineering, Faculty of Engineering, University of Sistan and Baluchestan, Zahedan, Iran*
[2]*Department of Civil Engineering, Faculty of Engineering, University of Birjand, Birjand, Iran*

(Received November 27, 2017, Revised May 10, 2018, Accepted July 10, 2018)

Abstract. The Dynamic equations in the polar coordinates are drawn out using the MLPG method for the non-symmetric FG cylindrical shell. To simulate the mechanical properties of FGM, the nonlinear volume fractions for radial direction are used. The shape function applied in this paper is a form of the radial basis functions, by using this function all the requirements for an effective and suitable shape function are established. Hence in this study, the multiquadrics (MQ) radial basis functions are exploited as the shape function governing the problem. The MLPG method is combined with the the Newmark time approximation scheme to solve dynamic equations in the time domain. The obtained results by the MLPG method to be verified are compared with the analytical solution and the FEM. The obtained results through the MLPG method show a good agreement in comparison to other results and the MLPG method has high accuracy for dynamic analysis of the non-symmetric FG cylindrical shell. To demonstrate the capability of the present method to dynamic analysis of the non-symmetric FG cylindrical shell, it is analyzed dynamically with different volume fraction exponents under harmonic and rectangular shock loading. The present method shows high accuracy, efficiency and capability to dynamic analysis of the non-symmetric FG cylindrical shell with nonlinear grading patterns.

Keywords: MLPG; cylindrical sell; FGM; dynamic analysis; volume fraction

1. Introduction

Dynamic analyses of cylindrical structure are one of the important engineering problems. The Functionally Graded Materials (FGMs) in cylindrical shell are used to optimize the displacements and stresses of structures. In this paper, the material properties of FGM are defined by nonlinear grading patterns. Chen *et al.* (2004a, b) a study on the vibration analysis of a functionally graded hollow cylinder presented. A frequency analysis was performed for Functionally Graded Material (FGM) circular cylindrical shells with various volume fraction laws by Arshad *et al.* (2007). Hosseini and Abolbashari (2010) and Hosseini *et al.* (2007) carried out dynamic analysis of functionally graded thick hollow cylinders. The gradient properties of functionally graded materials (FGMs) were taken as a volume fraction power-law distribution by Changcheng and Yinghui (2010). Khosravifard *et al.* (2011) focused on nonlinear transient heat conduction analysis of functionally graded materials. Stochastic wave propagation in functionally graded materials was studied by Hosseini and Shahabian (2011a, b). Rahimi *et al.* (2011) investigated the vibrational behavior of functionally graded cylindrical shells with intermediate ring supports. Buckling of functionally graded cylindrical shells under combined loads was perused by Huang *et al.* (2011). Ghannad *et al.* (2012) studied elastic analysis of pressurized thick truncated conical shells made of functionally graded materials. Axisymmetrical bending of single and multi-span functionally graded hollow cylinders was studied by Bian and Wang (2013). Xiang and Chen (2014) investigated meshless local collocation method for natural frequencies and mode shapes of laminated composite shells. Shen *et al.* (2014) proposed the beam-mode stability of periodic functionally graded material shells conveying fluid. Stress analysis in a 2D-FGM thick finite length hollow cylinder was performed by Najibi and Shojaeefard (2016). Vibration characteristics of FGM cylindrical shells resting on Pasternak elastic foundation were examined by Park and Kim (2016). Wu and Liu (2016) developed a state space meshless method for the 3D analysis of FGM axisymmetric circular plates. Free vibration analysis of rotating functionally graded cylindrical shells with orthogonal stiffeners was presented by Tu and Loi (2016).

In recent decades, meshless methods were well-developed and proposed as a new class of numerical methods. An extremely beneficial and efficient solving method in structures made of Functionally Graded Materials (FGMs) is Meshless Local Petrov-Galerkin (MLPG) method, because these materials have variable mechanical properties and this method doesn't require to the mesh generation on the domain, therefore we can continuously model these materials with this method. Analysis of thick plates by using a higher-order shear and normal deformable plate theory and MLPG

*Corresponding author, Assistant Professor
E-mail: mojtaba.mosavi@birjand.ac.ir
[a]Ph.D.
E-mail: yaser_sadeghi_83@yahoo.com
[b]Professor
E-mail: sohrabi@hamoon.usb.ac.ir

http://www.techno-press.com/journals/sem&subpage=7
ISSN: 1225-4568 (Print), 1598-6217 (Online)

method with radial basis functions was proposed by Xiao *et al.* (2007). They analyzed infinitesimal deformations of a homogeneous and isotropic thick elastic plate. They employed Radial Basis Functions (RBF) for constructing trial solutions and two types of RBFs, multiquadrics (MQ) and Thin Plate Splines (TPS), were utilized and effects of their shape parameters on the quality of the computed solution were examined for deformations of thick plates under different boundary conditions. Zhao *et al.* (2008) carried out geometric nonlinear analysis of plates and cylindrical shells via a linearly conforming radial point interpolation method. In their paper, Sander's nonlinear shell theory was utilized and the arc-length technique was used in conjunction with the modified Newton-Raphson method to solve the nonlinear equilibrium equations. The radial and polynomial basis functions were employed to construct the shape functions with Delta function property using a set of arbitrarily distributed nodes in local support domains. Akbari *et al.* (2010) studied analysis of thermoelastic waves in a two-dimensional functionally graded materials domain by the Meshless Local Petrov-Galerkin (MLPG) method. To investigate the effect of material composition on the dynamic response of functionally graded materials, a metal/ceramic composite was considered for which the transient thermal field, dynamic displacement and stress fields were reported for different material distributions. The thermo-elastic wave propagation based on Green-Naghdi (GN) coupled thermo-elasticity in a functionally graded thick hollow cylinder considering uncertainty in constitutive mechanical properties under thermal shock loading was investigated by Hosseini *et al.* (2011). The meshless local Petrov-Galerkin method accompanied with Monte-Carlo simulation was developed to solve the stochastic boundary value problem. Foroutan and Moradi (2011) surveyed dynamic analysis of functionally graded material cylinders under an impact load by a mesh-free method. In this analysis, Moving Least Square (MLS) shape functions were used for the approximation of the displacement field in the weak form of motion equation and essential boundary conditions were imposed by the transformation method. The resulting set of time domain differential equations was solved using central difference approximation. Rezaei Mojdehi *et al.* (2011) perused 3D static and dynamic analysis of thick functionally graded plates by the Meshless Local Petrov-Galerkin (MLPG) method. In their work, using the kinematics of a three dimensional continuum, the local weak form of the equilibrium equations was derived. A weak formulation for the set of governing equations was transformed into local integral equations on local sub-domains using a Heaviside step function as test function. Analysis of the bending of circular piezoelectric plates with functionally graded material properties by a MLPG method was studied by Sladek *et al.* (2013). In their work, material properties were considered to be continuously varying along the plate thickness, also the axial symmetry of geometry and boundary conditions for a circular plate reduced the original three-dimensional (3-D) boundary value problem into a two-dimensional (2-D) problem. Dynamic analysis of functionally graded nanocomposite cylinders reinforced by carbon nanotube by a mesh-free method was proposed by Moradi *et al.* (2013). In their paper, the free vibration and stress wave propagation behavior of carbon nanotube reinforced composite (CNTRC) cylinders were investigated. In this simulation, an axisymmetric model was used. Material properties were estimated by a micro mechanical model. Moving Least Squares (MLSs) shape functions were used for approximation of displacement field in the weak form of motion equation and the transformation method was exploited for the imposition of essential boundary conditions. Hosseini (2014) was perused application of Meshless Local Petrov-Galerkin (MLPG) and Generalized Finite Difference (GFD) methods in coupled thermoelasticity analysis of thick hollow cylinder. Ghadiri Rad *et al.* (2015) devoted their research to the geometrically nonlinear analysis of a functionally graded (FG) thick hollow cylinder with Rayleigh damping by using the meshless local Petrov–Galerkin (MLPG) method. At the end, to prove the robustness of the proposed method, several numerical tests are performed and effects of relative parameters on the dynamic behavior of the cylinder for various kinds of FGMs are discussed in detail. Findings demonstrate the effectiveness of the presented MLPG method for large deformation problems because of vanishing of the mesh distortion.

In this research, at first the equation governing the dynamic behavior of cylindrical shells made of functionally graded material derive in the polar coordinates using meshless local Petrov-Galerkin (MLPG) method. In order to discretize the derived equations in time domains, the Meshless Local Petrov-Galerkin (MLPG) method is combining with the Newmark time approximation scheme. The displacements can be approximated using shape function so that we choose radial functions as the basis in equation. The MLPG obtained results compare with analytical and Finite Element Method (FEM). At the end, the cylindrical shell under the harmonic and rectangular shock loading will be analyzed for the various values of volume fraction exponent and the results gained will be mentioned.

2. MLPG implementation

The governing dynamic equations of cylindrical shell with infinite length and asymmetric geometry and boundary conditions in polar coordinates can be written as follows

$$\sigma_{rr,r} + \frac{1}{r}\sigma_{r\theta,\theta} + \frac{1}{r}(\sigma_{rr} - \sigma_{\theta\theta}) = \rho(r)u_{r,tt} \tag{1}$$

$$\frac{1}{r}\sigma_{\theta\theta,\theta} + \sigma_{r\theta,r} + \frac{2}{r}\sigma_{r\theta} = \rho(r)u_{\theta,tt} \tag{2}$$

where, "σ_{rr}", "$\sigma_{\theta\theta}$" and "$\sigma_{r\theta}$" denote radial, hoop and shear stresses, respectively. "$\rho(r)$" is the mass density. The terms "u_r" and "u_θ" are the radial and hoop displacements, respectively.

The cylindrical shell made of FGM, and also FG material in this shell are graded through the r-direction. The material features of the FG cylindrical shell can be explained as

$$E(r) = E_c + (E_m - E_c)\left(\frac{r - r_{in}}{r_{out} - r_{in}}\right)^l \tag{3}$$

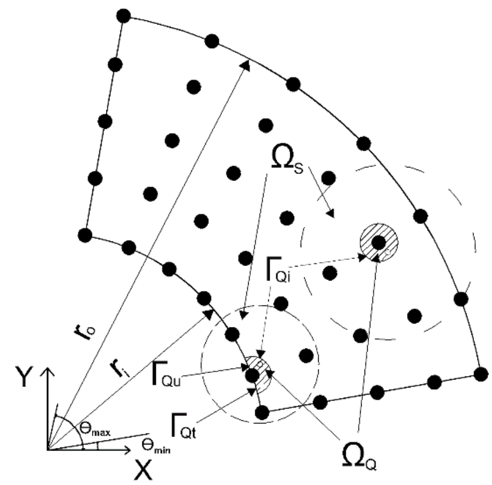

Fig. 1 The domain and the boundary of the cylindrical shell in the MLPG method

$$\rho(r) = \rho_c + (\rho_m - \rho_c)\left(\frac{r - r_{in}}{r_{out} - r_{in}}\right)^l \tag{4}$$

where, subscript "m" and "c" stand for metal and ceramic material, "E" and "ρ" are modulus of elasticity and mass density, respectively. "l" is a non-negative volume fraction exponent.

Constitutive equations for FG cylindrical are

$$\sigma_{ij} = D_{ijkl}\,\varepsilon_{kl} \tag{5}$$

$$D_{ijkl} = \mu\, D^0_{ijkl} \tag{6}$$

$$D^0_{ijkl} = \frac{2\nu}{(1-2\nu)}\delta_{ij}\delta_{kl} + \delta_{ik}\delta_{jl} + \delta_{il}\delta_{jk} \tag{7}$$

$$i, j, k, l = 1{,}2$$
$$\mu = \frac{E(r)}{2(1+\nu)} \tag{8}$$

where, "ν" is Poisson's ratio and "δ_{ij}" is Kronecker delta. The strain-displacement relations are following

$$\varepsilon_{rr} = u_{r,r} \tag{9}$$

$$\varepsilon_{\theta\theta} = \frac{1}{r}\left(u_{\theta,\theta} + u_r\right) \tag{10}$$

$$\varepsilon_{r\theta} = \frac{1}{r}u_{r,\theta} + u_{\theta,r} - \frac{1}{r}u_\theta \tag{11}$$

where "ε_{rr}", "$\varepsilon_{\theta\theta}$" and "$\varepsilon_{r\theta}$" are radial, hoop and shear strain, respectively. For the analysis of cylindrical shell with infinite length and asymmetric geometry and boundary conditions in polar coordinates, the following relation is used

$$d\Omega_s = r\, d\Omega \tag{12}$$

Based on the local weighted residual method, the weak-form for Eqs. (1)-(2) over a local subdomains Ω_Q (integration) instead of constructing the global weak-form for whole domain of dynamic problem can be stated as

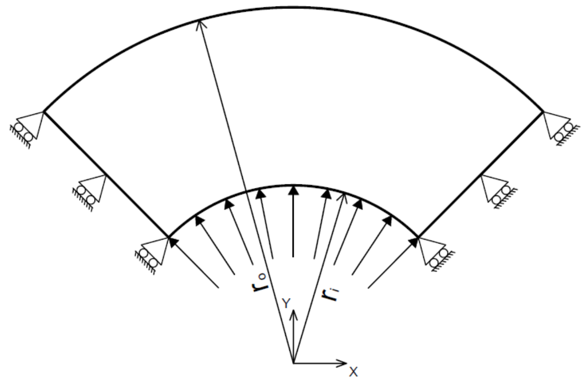

Fig. 2 The geometry and the boundary conditions of the cylinder

$$\int_{\Omega_Q} rW_I\left(\sigma_{rr,r} + \frac{(\sigma_{rr} - \sigma_{\theta\theta})}{r} + \frac{1}{r}\sigma_{r\theta,\theta} - \rho(r)u_{r,tt}\right)d\Omega = 0 \tag{13}$$

$$\int_{\Omega_Q} rW_I\left(\frac{1}{r}\sigma_{\theta\theta,\theta} + \sigma_{r\theta,r} + \frac{2\sigma_{r\theta}}{r} - \rho(r)u_{\theta,tt}\right)d\Omega = 0 \tag{14}$$

where "W_I" is the weight function and we use the same weight function for all the equations involved.

The divergence theory is employed for Eqs. (13)-(14) as follows, which "Ω_Q" and "Γ_Q" are quadrature domain and boundary of quadrature domain, respectively.

$$\int_{\Omega_Q}\left(rW_{I,r}\sigma_{rr} + W_I\sigma_{\theta\theta} + W_{I,\theta}\sigma_{r\theta}\right)d\Omega - \int_{\Gamma_Q} rW_I\left(n_r\sigma_{rr} + \frac{n_\theta}{r}\sigma_{r\theta}\right)d\Gamma 0 + \int_{\Omega_Q} rW_I\rho(r)u_{r,tt}\,d\Omega = 0 \tag{15}$$

$$\int_{\Omega_Q}\left(W_{I,\theta}\sigma_{\theta\theta} + rW_{I,r}\sigma_{r\theta} - W_I\sigma_{r\theta}\right)d\Omega - \int_{\Gamma_Q} rW_I\left(\frac{n_\theta}{r}\sigma_{\theta\theta} + n_r\sigma_{r\theta}\right)d\Gamma + \int_{\Omega_Q} rW_I\rho(r)u_{\theta,tt}\,d\Omega = 0 \tag{16}$$

where "n_r" and "n_θ" are the unit outward normal vector on the boundary for "r" and "θ" direction, respectively.

The boundary of quadrature domain is divided to some parts as "$\Gamma_Q = \Gamma_{Q_i} \cup \Gamma_{Q_u} \cup \Gamma_{Q_t}$". The term "$\Gamma_{Q_i}$" is the internal boundary of the quadrature domain, "Γ_{Q_u}" is the part of the essential boundary that intersects with the quadrature domain and "Γ_{Q_t}" is the part of the natural boundary that intersects with the quadrature domain (see Fig. 1).

We can then change the expression of Eqs. (15)-(16) to

$$\begin{aligned}\int_{\Omega_Q} \left(rW_{I,r}\sigma_{rr} + W_I\sigma_{\theta\theta} + W_{I,\theta}\sigma_{r\theta}\right) d\Omega \\ - \int_{\Gamma_{Q_i}} rW_I\left(n_r\sigma_{rr} + \frac{n_\theta}{r}\sigma_{r\theta}\right) d\Gamma \\ - \int_{\Gamma_{Qu}} rW_I\left(n_r\sigma_{rr} + \frac{n_\theta}{r}\sigma_{r\theta}\right) d\Gamma \\ + \int_{\Omega_Q} rW_I\rho(r)u_{r,tt}\, d\Omega \\ = \int_{\Gamma_{Q_t}} rW_I t_r\, d\Gamma\end{aligned} \tag{17}$$

$$\begin{aligned}\int_{\Omega_Q} \left(W_{I,\theta}\sigma_{\theta\theta} + rW_{I,r}\sigma_{r\theta} - W_I\sigma_{r\theta}\right) d\Omega \\ - \int_{\Gamma_{Q_i}} rW_I\left(\frac{n_\theta}{r}\sigma_{\theta\theta} + n_r\sigma_{r\theta}\right) d\Gamma \\ - \int_{\Gamma_{Qu}} rW_I\left(\frac{n_\theta}{r}\sigma_{\theta\theta} + n_r\sigma_{r\theta}\right) d\Gamma \\ + \int_{\Omega_Q} rW_I\rho(r)u_{\theta,tt}\, d\Omega \\ = \int_{\Gamma_{Q_t}} rW_I t_\theta\, d\Gamma\end{aligned} \tag{18}$$

where "t_r" and "t_θ" are the radial and hoop tractions, respectively and they are defined as follows

$$t_r = n_r\sigma_{rr} + \frac{n_\theta}{r}\sigma_{r\theta} \tag{19}$$

$$t_\theta = n_r\sigma_{r\theta} + \frac{n_\theta}{r}\sigma_{\theta\theta} \tag{20}$$

The matrix form of Eqs. (17)-(18) is given as

$$\begin{aligned}\int_{\Omega_Q} \widehat{\boldsymbol{V}}_{\boldsymbol{I}}\boldsymbol{\sigma}\, d\Omega - \int_{\Gamma_{Q_i}} r\boldsymbol{W_I n\,\sigma}\, d\Gamma - \int_{\Gamma_{Qu}} r\boldsymbol{W_I n\,\sigma}\, d\Gamma \\ + \int_{\Omega_Q} r\boldsymbol{W_I}\rho\boldsymbol{u}_{,tt}\, d\Omega = \int_{\Gamma_{Q_t}} r\boldsymbol{W_I}\bar{\boldsymbol{t}}\; d\Gamma\end{aligned} \tag{21}$$

where "$\widehat{\boldsymbol{V}}_{\boldsymbol{I}}$", "$\boldsymbol{\sigma}$", "$\boldsymbol{W_I}$", "$\boldsymbol{n}$" and "$\bar{\boldsymbol{t}}$" are the derivative of weight function, the stress vector, matrix of weight functions, matrix of unit outward normal and traction vector, respectively, which are as follows

$$\widehat{\boldsymbol{V}}_{\boldsymbol{I}} = \begin{bmatrix} rW_{I,r} & W_I & W_{I,\theta} \\ 0 & W_{I,\theta} & rW_{I,r} - W_I \end{bmatrix} \tag{22}$$

$$\boldsymbol{\sigma}^T = \{\sigma_{rr} \quad \sigma_{\theta\theta} \quad \sigma_{r\theta}\} \tag{23}$$

$$\boldsymbol{W_I} = \begin{bmatrix} W_I & 0 \\ 0 & W_I \end{bmatrix} \tag{24}$$

$$\boldsymbol{n} = \begin{bmatrix} n_r & 0 & \dfrac{n_\theta}{r} \\ 0 & \dfrac{n_\theta}{r} & n_r \end{bmatrix} \tag{25}$$

$$\bar{\boldsymbol{t}} = \begin{Bmatrix} t_r \\ t_\theta \end{Bmatrix} \tag{26}$$

The displacements can be approximated using shape function. Shape function is defined for each point using the nodes in support domain "Ω_s" of a point (see Fig. 1). In this paper, we use the Radial Point Interpolation Method (RPIM) shape function, the advantage of using this shape function is its simpleness and high precision. We choose radial functions as the basis in equation

$$u_r(r,\theta,t) = u_r(\bar{r},t) = \varphi(\bar{r})\,\bar{u}_r(t) \tag{27}$$

$$u_\theta(r,\theta,t) = u_\theta(\bar{r},t) = \varphi(\bar{r})\,\bar{u}_\theta(t) \tag{28}$$

The matrix form of Eqs. (27)-(28) can be assessed as

$$u = \begin{Bmatrix} u_r \\ u_\theta \end{Bmatrix} = \sum_{j=1}^{k} \begin{bmatrix} \varphi_j & 0 \\ 0 & \varphi_j \end{bmatrix} \begin{Bmatrix} u_{rj} \\ u_{\theta j} \end{Bmatrix} = \sum_{j=1}^{k} \boldsymbol{\Phi_j}\,\boldsymbol{u_j} \tag{29}$$

"$\bar{r}$" is distance between point "x" and "x_I", so we have

$$\bar{r} = \sqrt{r^2 + r_I^2 - 2r\,r_I\cos(\theta - \theta_I)} \tag{30}$$

Furthermore, shape function "$\varphi(\bar{r})$" is defined as follows

$$\varphi(\bar{r}) = R^T(\bar{r})\,R_Q^{-1} \tag{31}$$

The vector "R" and matrix "R_Q" can be written

$$R^T(\bar{r}) = \{R_1(\bar{r}) \quad R_2(\bar{r}) \quad \dots \quad R_n(\bar{r})\} \tag{32}$$

$$R_Q = \begin{bmatrix} R_1(\bar{r}_1) & R_2(\bar{r}_1) & \dots & R_n(\bar{r}_1) \\ R_1(\bar{r}_2) & R_2(\bar{r}_2) & \dots & R_n(\bar{r}_2) \\ \vdots & \vdots & \ddots & \vdots \\ R_1(\bar{r}_n) & R_2(\bar{r}_n) & \dots & R_n(\bar{r}_n) \end{bmatrix} \tag{33}$$

There are a number of forms of radial basis functions used by the mathematics community. In this paper we use the type of a classical form called multiquadric (MQ) basis. The MQ basis function is following

$$R_i(\bar{r}) = (\bar{r}^2 + C^2)^q \tag{34}$$

where "C" and "q" are constant coefficient.

Substitution of the Eqs. (5) and (29) into Eq. (21) gives

$$\int_{\Omega_Q} \widehat{\boldsymbol{V}}_I \boldsymbol{D} \sum_{j=1}^{k} \boldsymbol{B}_j \boldsymbol{u}_j \, d\Omega - \int_{\Gamma_{Q_i}} r \boldsymbol{W}_I \boldsymbol{n} \boldsymbol{D} \sum_{j=1}^{k} \boldsymbol{B}_j \boldsymbol{u}_j \, d\Gamma - \int_{\Gamma_{Qu}} r \boldsymbol{W}_I \boldsymbol{n} \boldsymbol{D} \sum_{j=1}^{k} \boldsymbol{B}_j \boldsymbol{u}_j \, d\Gamma + \int_{\Omega_Q} r \boldsymbol{W}_I \rho(r) \sum_{j=1}^{k} \boldsymbol{\Phi}_j \boldsymbol{u}_{j,tt} \, d\Omega = \int_{\Gamma_{Qt}} r \boldsymbol{W}_I \bar{\boldsymbol{t}} \, d\Gamma \tag{35}$$

where "k" is the number of nodes. Matrix "$\boldsymbol{D}$" and "$\boldsymbol{B}$" are defined as follows

$$\boldsymbol{D} = \frac{E(r)}{(1+\nu)(1-2\nu)} \begin{bmatrix} 1-\nu & \nu & 0 \\ \nu & 1-\nu & 0 \\ 0 & 0 & \dfrac{1-2\nu}{2} \end{bmatrix} \tag{36}$$

$$\boldsymbol{B_j} = \begin{bmatrix} \varphi_{j,r} & 0 \\ \dfrac{\varphi_j}{r} & \dfrac{1}{r}\varphi_{j,\theta} \\ \dfrac{1}{r}\varphi_{j,\theta} & \varphi_{j,r} - \dfrac{\varphi_j}{r} \end{bmatrix} \tag{37}$$

There are some numerical techniques to solve the governing equations in time domain. In this article, the Newmark time approximation scheme is used for time domain analysis with the initial conditions that they are assumed to be zero. Consider the governing equation of non-dimensional time $\bar{t} = t_p$ of system takes the form

$$[M]\{\ddot{u}^{t_p}\} + [K]\{u^{t_p}\} = \{F^{t_p}\} \tag{38}$$

F^0 and u^0, are the initial conditions so the following equation can be obtained

$$[M]\{\ddot{u}^0\} = \{F^0\} - [K]\{u^0\} \tag{39}$$

The matrices $[K_m]$ and the vector $\left\{F_m^{t_p}\right\}$ are specified as follows

$$[K_m] = [K] + \frac{1}{\lambda_1 \Delta t^2}[M] \tag{40}$$

$$\left\{F_m^{t_p}\right\} = \{F^{t_p}\} + \frac{1}{\lambda_1 \Delta t^2}[M](\{u^{t_p-1}\} + \Delta t\{\dot{u}^{t_p-1}\} + (0.5-\lambda_1)\Delta t^2\{\ddot{u}^{t_p-1}\}) \tag{41}$$

Using following equations the matrices of $[u^{t_p}]$, $[\dot{u}^{t_p}]$, and $[\ddot{u}^{t_p}]$ can be calculated

$$\{u^{t_p}\} = [K_m]^{-1}\left\{f_m^{t_p}\right\} \tag{42}$$

$$\{\ddot{u}^{t_p}\} = \frac{1}{\lambda_1 \Delta t^2}(\{u^{t_p}\} - \{u^{t_p-1}\} - \Delta t\{\dot{u}^{t_p-1}\} - \Delta t^2(0.5-\lambda_1)\{\ddot{u}^{t_p-1}\}) \tag{43}$$

$$\{\dot{u}^{t_p}\} = \{\dot{u}^{t_p-1}\} + \Delta t[(1-\lambda_2)\{\ddot{u}^{t_p-1}\} + \lambda_2\{\ddot{u}^{t_p}\}] \tag{44}$$

Using aforementioned equations, the matrices of $\{u^{t_p}\}$, $\{\dot{u}^{t_p}\}$, and $\{\ddot{u}^{t_p}\}$ can be gained for an arbitrary time. The best convergence rate can be attained in this method by choosing

$$\lambda_1 = 1/4 \text{ and } \lambda_2 = 1/2 \tag{45}$$

3. Verification

In numerical methods, assurance of the accuracy of the results obtained is very important. For the comparison purpose, the current results of the dynamic behavior of a FG cylindrical shell are compared with those obtained using the analytical and FEM methods in the following examples.

3.1 Verification with analytical solution

In this section, a cylindrical shell with infinite length is analyzed using MLPG method and the results are compared with analytical solution. The following boundary conditions were assumed for the verified problem.

$$\begin{aligned} &\sigma_r(r_i,\theta,t) = P(t) && \sigma_r(r_o,\theta,t) = 0 \\ &\sigma_\theta(r_i,\theta,t_0) = 0 && \sigma_\theta(r_o,\theta,t_0) = 0 \\ &\tau_{r\theta}(r_i,\theta,t) = 0 && \tau_{r\theta}(r_o,\theta,t) = 0 \\ &u_r(r,\theta_{min},t_0) = 0 && u_r(r,\theta_{max},t_0) = 0 \\ &u_\theta(r,\theta_{min},t) = 0 && u_\theta(r,\theta_{max},t) = 0 \end{aligned} \tag{46}$$

$$P(t) = P_0(1 - e^{-c_0 t}) \tag{47}$$

where $P_0 = 20\,MPa$ and $c_0 = 10^2 \frac{1}{sec}$ are assumed. The Eq. (47) for the long time approaches to P_0 slowly, so the dynamic analysis can be similar to the static analysis, furthermore it can be used for analytical solution of loading radial stress, hoop stress and radial displacement (Ugural and Fenster 2003) obtained as follows

$$\sigma_{rr} = \frac{r_{in}^2 r_{out}^2 (P_{out} - P_{in})}{r_{out}^2 - r_{in}^2}\frac{1}{r^2} + \frac{r_{in}^2 P_{in} - r_{out}^2 P_{out}}{r_{out}^2 - r_{in}^2} \tag{48}$$

$$\sigma_{\theta\theta} = -\frac{r_{in}^2 r_{out}^2 (P_{out} - P_{in})}{r_{out}^2 - r_{in}^2}\frac{1}{r^2} + \frac{r_{in}^2 P_{in} - r_{out}^2 P_{out}}{r_{out}^2 - r_{in}^2} \tag{49}$$

$$u_{rr} = \frac{1+\nu}{E}\left[\frac{r_{in}^2 r_{out}^2 (P_{out} - P_{in})}{r_{out}^2 - r_{in}^2}\frac{1}{r} + (1-2\nu)\frac{r_{in}^2 P_{in} - r_{out}^2 P_{out}}{r_{out}^2 - r_{in}^2} r\right] \tag{50}$$

So, a cylinder with infinite length is presumed, in which $r_i = 0.25\,m$, $r_o = 0.5\,m$ and $\theta = {}^{\pi}/_{2}\ rad$, are supposed as the inner, outer radius, and angle of cylinder, respectively. The geometry of this cylinder is demonstrated in Fig. 2.

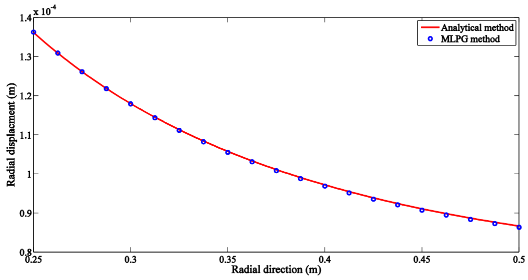

Fig. 3 The obtained results through the MLPG method in comparison with those acquired using analytical method for radial displacement

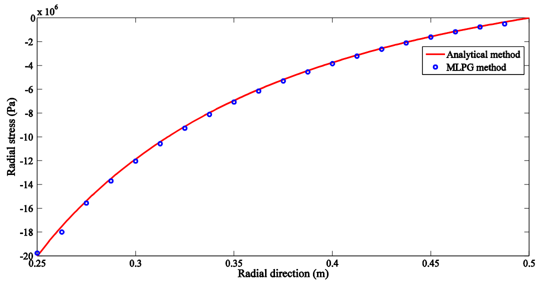

Fig. 4 The obtained results through the MLPG method in comparison with those acquired using analytical method for radial stress

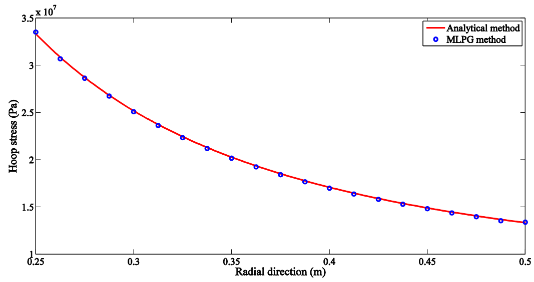

Fig. 5 The obtained results through the MLPG method in comparison with those acquired using analytical method for hoop stress

Table 1 The obtained results through the MLPG method in comparison with those acquired using analytical method for middle point of thickness of the cylinder

	Analytical method (Ugural and Fenste 2003)	MLPG method	percentage error
Radial displacement (m)	1.0111×10^{-4}	1.0112×10^{-4}	9.89×10^{-3}
Radial stress (Pa)	-5.185×10^{6}	-5.139×10^{6}	0.8872
Hoop stress (Pa)	1.852×10^{7}	1.842×10^{7}	0.5399

The comparison of the results procured using the meshless method with those gained through the analytical solution is shown in Figs. 3-5. As can be seen in these figures, the results of the meshless method have passable accordance to the results of the analytical solution.

Table 2 The mechanical properties of the FG cylindrical shell

Material location	Elastic modulus	Poisson's ratio	Mass density
Outer radius	$70\ GPa$	0.3	$2707\ kg/m^3$
inner radius	$380\ GPa$	0.3	$3800\ kg/m^3$

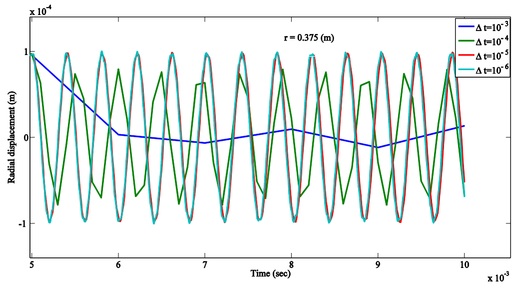

Fig. 6 The converging trend of the radial displacement with different time steps

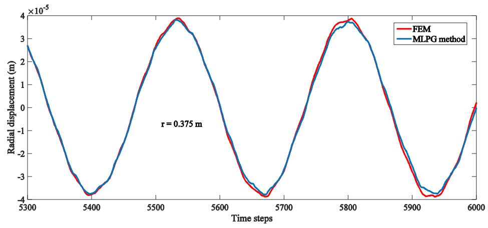

Fig. 7 The obtained results through the MLPG method in comparison with those acquired using the FEM for the radial displacement

In Table 1, percentage errors for local Petrov-Galerkin method and the analytical solution in middle point of thickness of the cylinder $(r = 0.375\ m)$ are indicated. Table 1 depicts the relation accomplished with local Petrov–Galerkin method has very high accuracy, thus this method can be exploited as a practical approach for dynamic analysis of cylindrical shell.

3.2 Verification with FEM

In this section, in order to verify the accuracy of local Petrov-Galerkin method and also for demonstrating the ability of the present method in the analysis of structures made of functionally graded material, a cylindrical shell is simulated under the shock loading. The obtained results of this method are compared with the finite element method (FEM) (Shakeri *et al.* 2006).

For verification, a cylinder with the inner radius $r_{in} = 0.25\ m$ and the outer radius $r_{out} = 0.5\ m$ made of functionally graded material with the mechanical properties presented in Table 2 is considered.

The cylinder is under shock loading as follows

$$P(t) = \begin{cases} P_0 t & t \leq 0.005\ sec \\ 0 & t > 0.005\ sec \end{cases} \tag{51}$$

where $P_0 = 4\ GPa/sec$. In this problem for choosing the appropriate time step, many analyses carry out. These results can be seen in Fig. 6. From this figure is concluded the best

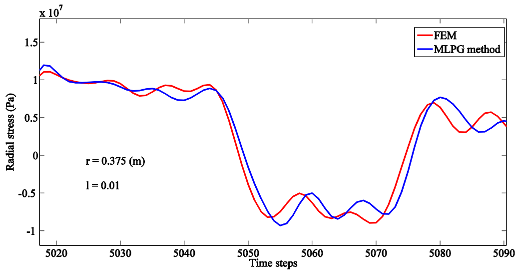

Fig. 8 The obtained results through the MLPG method in comparison with those acquired using the FEM for the radial stress

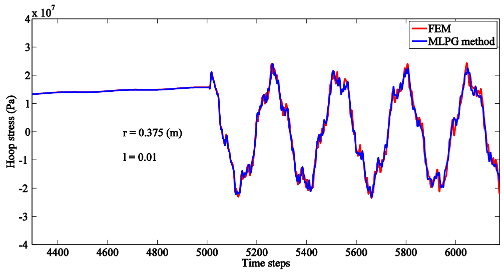

Fig. 9 The obtained results through the MLPG method in comparison with those acquired using the FEM for the hoop stress

Table 3 The obtained results through the MLPG method in comparison with those acquired using the finite element method for middle point of thickness of the cylinder at time step 520

	FEM (Shakeri *et al.* 2006)	MLPG method	Percentage difference
Radial displacement (m)	-9.465×10^{-5}	-9.466×10^{-5}	0.011
Radial stress (Pa)	-9.885×10^{6}	-9.779×10^{6}	1.072
Hoop stress (Pa)	-2.441×10^{7}	-2.421×10^{7}	0.819

time step is $\Delta t = 10^{-5}\ sec$.The obtained results with MLPG method show a passable accordance in comparison with other results (Figs. 7-9). The acquired results illustrate until time step 5000 the cylindrical shell is under loading and then the load is missed suddenly, therefore the cylindrical shell starts the free vibration. The obtained percentage difference for radial displacement, radial stress and hoop stress are represented in Table 3. As can be seen from Table 3, the MLPG method has high accuracy for dynamic analysis of the cylindrical shell.

4. Numerical results and discussion

At this level, we analyzed the cylinder dynamically with different volume fraction exponents using the MLPG method under harmonic and rectangular shock loading, in order to evaluating capability of this method for dynamic analysis of the FG cylindrical shell.

4.1 Harmonic shock loading

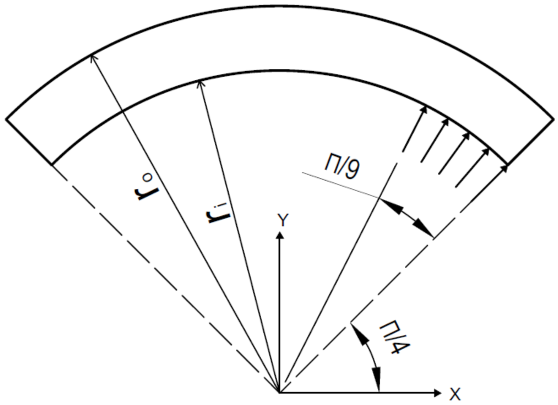

Fig. 10 The geometry and the boundary conditions under shock loading

To assess the sufficiency of the MLPG method, a non-symmetric FG cylinder with the inner radius $r_i = 0.25\,m$, the outer radius $r_o = 0.5\,m$, minimum and maximum angle of cylinder $\theta_{min} = {}^{\pi}/_{4}\ rad$ and $\theta_{max} = {}^{3\pi}/_{4}\ rad$ with the mechanical properties exhibited in Table 2 is assumed (see Fig. 10). The boundary conditions and the loading are as follows

$$\begin{aligned} &\sigma_r(r_i,\theta,t) = P(t) && \sigma_r(r_o,\theta,t) = 0 \\ &\sigma_\theta(r_i,\theta,t_0) = 0 && \sigma_\theta(r_o,\theta,t_0) = 0 \\ &\tau_{r\theta}(r_i,\theta,t) = 0 && \tau_{r\theta}(r_o,\theta,t) = 0 \\ &u_r(r,\theta_{min},t) = 0 && u_r(r,\theta_{max},t) = 0 \\ &u_\theta(r,\theta_{min},t) = 0 && u_\theta(r,\theta_{max},t) = 0 \end{aligned} \tag{52}$$

$$P(t) = \begin{cases} P_0\sin(c_0 t) & t \le 0.005\ \text{sec} \quad \dfrac{\pi}{4} \le \theta \le \dfrac{13\pi}{36} \\ 0 & t > 0.005\ \text{sec} \quad \theta > \dfrac{13\pi}{36} \end{cases} \tag{53}$$

where $c_0 = 15\times10^3\ \frac{1}{sec}$ and $P_0 = 10\ MPa$.

In Figs. 11-15 are depicted radial and hoop displacements and radial, hoop and shear stresses at $r = 0.375\ m$ and $\theta = \frac{\pi}{2}\ rad$ for various values of volume fraction exponent. It is concluded that the radial and hoop displacements maximum amplitude decrease and the structure frequency is raised (Figs. 11-12) by increasing the value of volume fraction exponent, also the similar behaviors can be seen for hoop stress (see Fig. 13). Fig. 14 shows by increasing the value of volume fraction exponent, the maximum amplitude of radial stress does not have much difference. The clear trend cannot be seen for the shear stress with the various values of volume fraction exponent, thereupon the maximum value of shear stress happens for $l = 0.75$ (see Fig. 15).

One of the most advantages of the presented meshless method is its application for analysis of two dimensions wave propagation in polar coordinate. The 2D wave propagation of radial and hoop stresses in 2D domain are illustrated in Figs. 16-17. These figures depict the

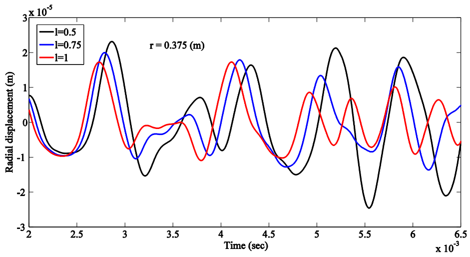

Fig. 11 The time history of the radial displacement for $l = 0.5$, $l = 0.75$ and $l = 1$ under the harmonic shock loading

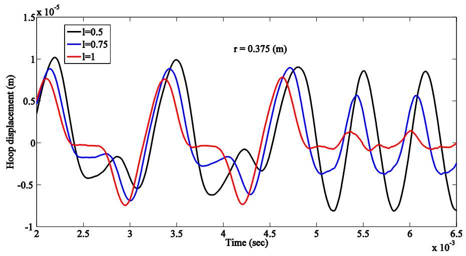

Fig. 12 The time history of the hoop displacement for $l = 0.5$, $l = 0.75$ and $l = 1$ under the harmonic shock loading

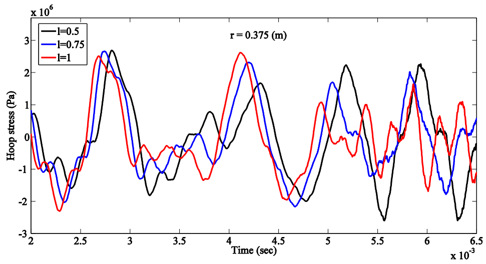

Fig. 13 The time history of the hoop stress for $l = 0.5$, $l = 0.75$ and $l = 1$ under the harmonic shock loading

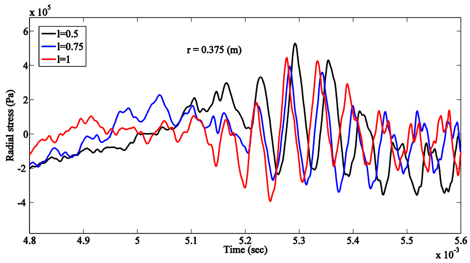

Fig. 14 The time history of the radial stress for $l = 0.5$, $l = 0.75$ and $l = 1$ under the harmonic shock loading

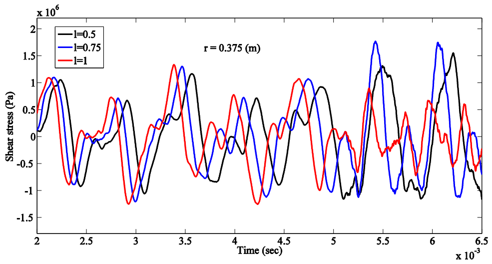

Fig. 15 The time history of the shear stress for $l = 0.5$, $l = 0.75$ and $l = 1$ under the harmonic shock loading

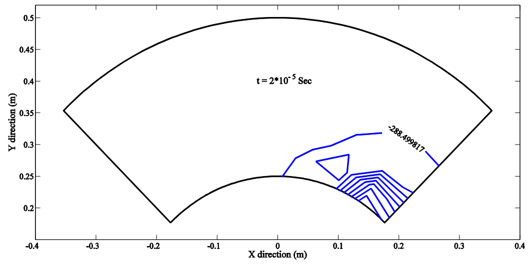

(a) $t = 2\times10^{-5}$ sec

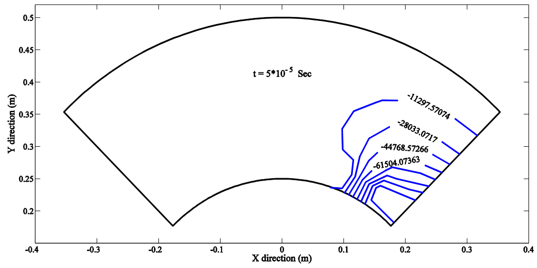

(b) $t = 5\times10^{-5}$ sec

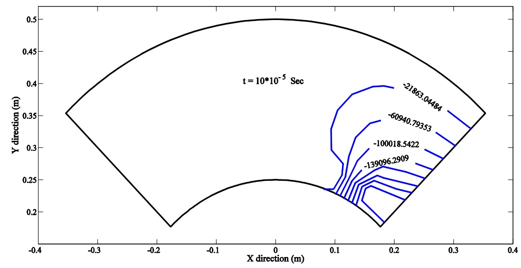

(c) $t = 10\times10^{-5}$ sec

Fig. 16 Two dimensional radial stress wave propagation at various times under the harmonic shock loading

propagation of radial and hoop stresses wave at different time. From these figures can be seen how wave move in structure in different time.

4.2 Rectangular shock loading

The same geometry and boundary conditions with problem 4.1 are assumed for a non-symmetric FG cylinder under rectangular shock loading. Table 2 shows the material properties for the FG cylinder. The loading is supposed as follows

$$P(t) = \begin{cases} P_0 & t \leq 0.005\,\text{sec} \quad \dfrac{\pi}{4} \leq \theta \leq \dfrac{13\pi}{36} \\ 0 & t > 0.005\text{sec} \qquad \theta > \dfrac{13\pi}{36} \end{cases} \tag{54}$$

where $P_0 = 15\ MPa$ is considered. Figs. 18-22 illustrate the radial and hoop displacements and radial, hoop and shear stresses. The maximum amplitude of the radial and hoop displacements (Figs. 18-19) by increasing the value of volume fraction exponent have decreased, such that, the radial displacement increases after exerting the impact loading within the confines of free vibration for $l = 0.5$,suddenly (Fig. 18). After applying the impact loading in the

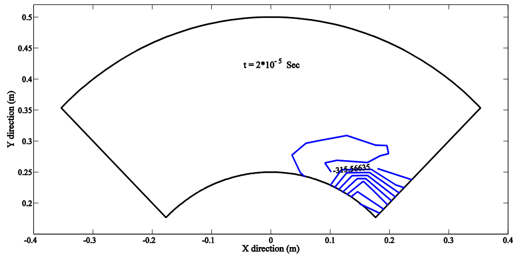

(a) $t = 2\times10^{-5}$ sec

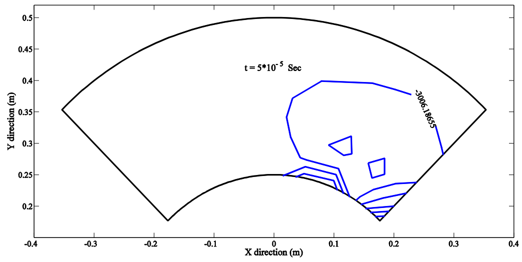

(b) $t = 5\times10^{-5}$ sec

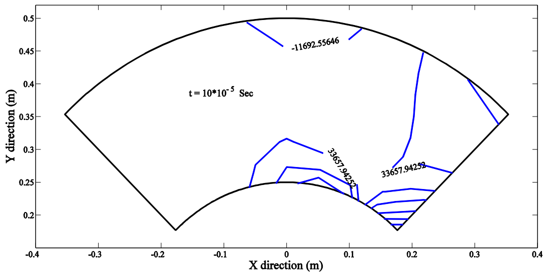

(c) $t = 10\times10^{-5}$ sec

Fig. 17 Two dimensional hoop stress wave propagation at various times under the harmonic shock loading

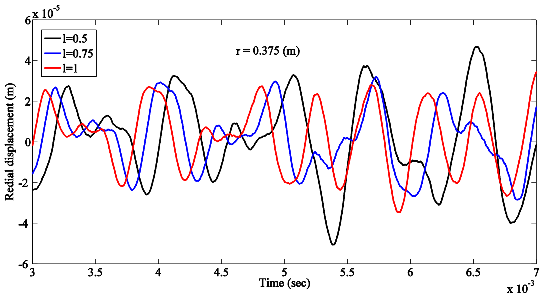

Fig. 18 The time history of the radial displacement for $l = 0.5$, $l = 0.75$ and $l = 1$ under the rectangular shock loading

range of free vibration for $l = 0.5$ and $l = 0.75$, the peak hoop displacement escalates and this trend for $l = 1$ is inverse. It can be realized from Fig. 20 that the maximum radial stress occurs for $l = 0.75$. In Fig. 21 is seen the maximum hoop stress rises by increasing the value of volume fraction exponent. Within the confines of free vibration in comparison with forced vibration, the value of hoop stress has a significant growth. The maximum of shear stress occurs in the range of free vibration for $l = 0.75$ (see Fig. 22).

The 2D wave propagation of radial and hoop stresses

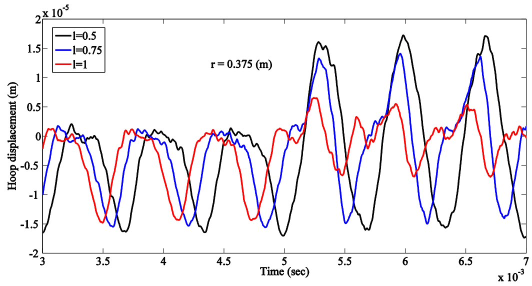

Fig. 19 The time history of the hoop displacement for $l = 0.5$, $l = 0.75$ and $l = 1$ under the rectangular shock loading

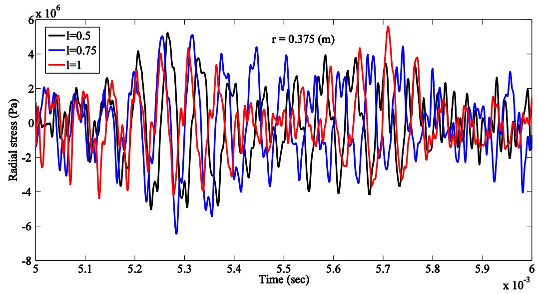

Fig. 20 The time history of the radial stress for $l = 0.5$, $l = 0.75$ and $l = 1$ under the rectangular shock loading

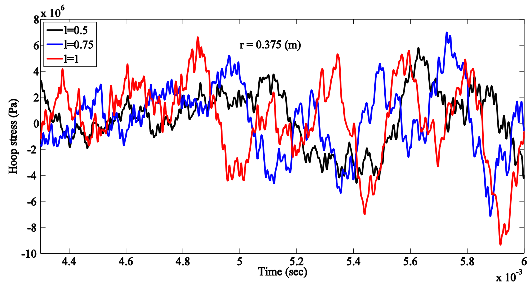

Fig. 21 The time history of the hoop stress for $l = 0.5$, $l = 0.75$ and $l = 1$ under the rectangular shock loading

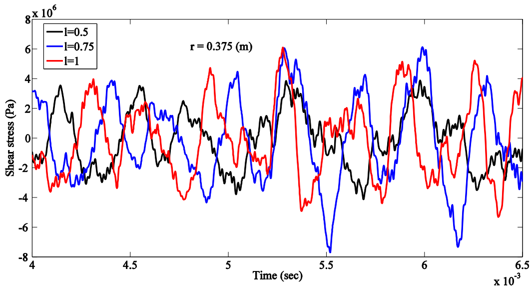

Fig. 22 The time history of the shear stress for $l = 0.5$, $l = 0.75$ and $l = 1$ under the rectangular shock loading

under rectangular shock loading in 2D domain are showed in Figs. 23-24 is displayed. These figures depict the propagation of radial and hoop stresses wave at different time. From these figures can see how wave move in structure in different time.

5. Conclusions

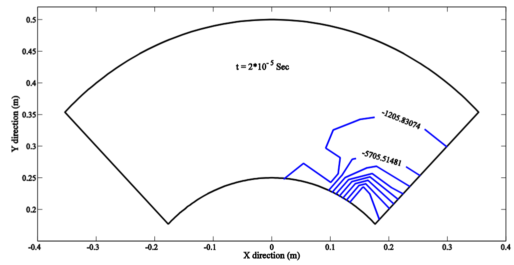

(a) $t = 2\times10^{-5}$ sec

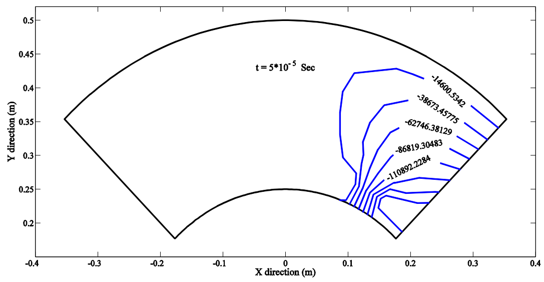

(b) $t = 5\times10^{-5}$ sec

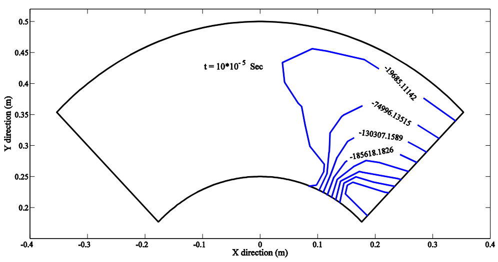

(c) $t = 10\times10^{-5}$ sec

Fig. 23 Two dimensional radial stress wave propagation at various times under the rectangular shock loading

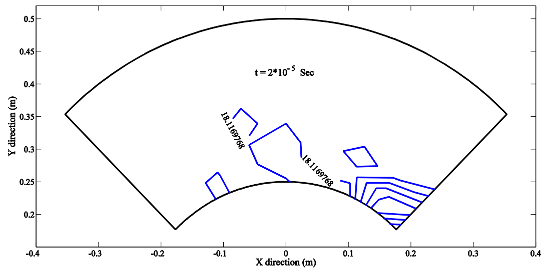

(a) $t = 2\times10^{-5}$ sec

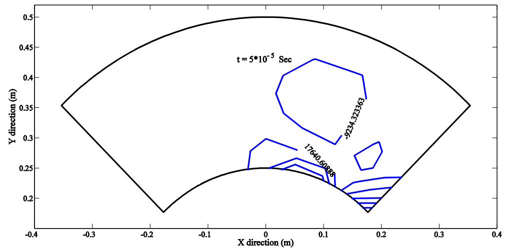

(b) $t = 5\times10^{-5}$ sec

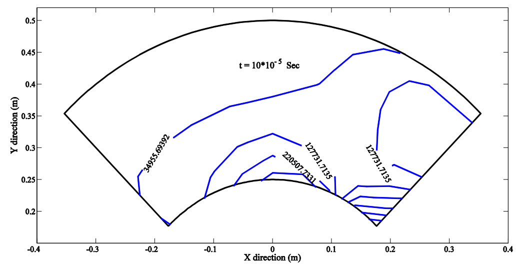

(c) $t = 10\times10^{-5}$ sec

Fig. 24 Two dimensional hoop stress wave propagation at various times under the rectangular shock loading

In the current study, meshless local Petrov-Galerkin (MLPG) method is developed for dynamic analysis of the non-symmetric FG cylindrical shell and assessment of stress wave propagation. Nonlinear volume fractions have been used in the direction of radius to simulate the mechanical properties of FGM. Newmark finite difference (NFD) method is combined with the meshless local Petrov-Galerkin (MLPG) method to obtain the dynamic behaviors. The inner surface of 2D-FG cylindrical panel is excited by suddenly unloading as mechanical shock loading. The major conclusions resulting from the above analysis can be summarized as follows:

• The effects of various grading patterns of mechanical properties on dynamic behaviors are studied in details for 2D-FG cylindrical shell using the presented hybrid meshless technique.

• The obtained results with MLPG method indicate a passable accordance in comparison to the acquired results of analytical method and FEM. In fact, this issue expresses the high precision and ability of the MLPG method for dynamic analysis of the non-symmetric FG cylindrical shell.

• The convergence of the present method for two dimensional dynamic analysis of 2D-FG cylindrical shell have been tested.

• The stress wave propagations are obtained in 2D domain as some contours at various time instants.

• By using the presented method, it is possible to track the different stress wave fronts in two dimensional domains for various volume fraction exponents.

• The present analysis furnishes a ground for natural frequency analysis of FGMs with two dimensional grading patterns.

References

Akbari, A., Bagri, A., Bordas, S. and Rabczuk, T. (2010), “Analysis of thermoelastic waves in a two-dimensional functionally graded materials domain by the meshless local Petrov-Galerkin (MLPG) method”, *Comput. Model. Eng. Sci.*, **65**, 27-74.

Arshad, S.H., Naeem, M.N. and Sultana, N. (2007), “Frequency analysis of functionally graded material cylindrical shells with various volume fraction laws”, *J. Mech. Eng. Sci.*, **221**, 1483-1495.

Bian, Z.G. and Wang, Y.H. (2013), “Axisymmetrical bending of single- and multi-span functionally graded hollow cylinders”, *Struct. Eng. Mech.*, **45**, 355-371.

Changcheng, D. and Yinghui, L. (2010), "Vibration characteristic analysis of functionally graded cylindrical thin shells", *Proceedings of the 2nd International Conference on Mechanical and Electrical Technology*, Singapore, September.

Chen, W.Q., Bian, Z.G. and Ding, H.J. (2004a), "Three-dimensional vibration analysis of fluid-filled orthotropic FGM cylindrical shells", *Int. J. Mech. Sci.*, **46**, 159-171.

Chen, W.Q., Bian, Z.G., Lv, C.F. and Ding, H.J. (2004b), "3D free vibration analysis of a functionally graded piezoelectric hollow cylinder filled with compressible fluid", *Int. J. Sol. Struct.*, **41**, 947-964.

Foroutan, M. and Moradi-Dastjerdi, R. (2011), "Dynamic analysis of functionally graded material cylinders under an impact load by a mesh-free method", *Acta Mech.*, **219**, 281-290.

Ghadiri Rad, M.H., Shahabian, F. and Hosseini, S.M. (2015), "A meshless local Petrov-Galerkin method for nonlinear dynamic analyses of hyper-elastic FG thick hollow cylinder with Rayleigh damping", *Acta Mech.*, **226**(5), 1497-1513.

Ghannad, M., Zamani Nejad, M., Rahimi, G.H. and Sabouri, H. (2012), "Elastic analysis of pressurized thick truncated conical shells made of functionally graded materials", *Struct. Eng. Mech.*, **43**, 105-126.

Hosseini, S.M. (2014), "Application of meshless local Petrov-Galerkin (MLPG) and generalized finite difference (GFD) methods in coupled thermoelasticity analysis of thick hollow cylinder", *Encyclop. Therm. Stress.*, **41**, 216-224.

Hosseini, S.M. and Abolbashari, M.H. (2010), "General analytical solution for elastic radial wave propagation and dynamic analysis of functionally graded thick hollow cylinders subjected to impact loading", *Acta Mech.*, **212**, 1-19.

Hosseini, S.M. and Shahabian, F. (2011a), "Stochastic assessment of thermo-elastic wave propagation in functionally graded materials (FGMs) with Gaussian uncertainty in constitutive mechanical properties", *J. Therm. Stress.*, **34**, 1071-1099.

Hosseini, S.M. and Shahabian, F. (2011b), "Transient analysis of thermo-elastic waves in thick hollow cylinders using a stochastic hybrid numerical method, considering Gaussian mechanical properties", *Appl. Math. Modell.*, **35**, 4697-4714.

Hosseini, S.M., Akhlaghi, M. and Shakeri, M. (2007), "Dynamic response and radial wave propagation velocity in thick hollow cylinder made of functionally graded materials", *Eng. Comput.*, **24**, 288-303.

Hosseini, S.M., Shahabian, F., Sladek, J. and Sladek, V. (2011), "Stochastic meshless local Petrov-Galerkin (MLPG) method for thermo-elastic wave propagation analysis in functionally graded thick hollow cylinders", *Comput. Model. Eng. Sci.*, **71**(1), 39-66.

Huang, H., Han, Q., Feng, N. and Fan, X. (2011), "Buckling of functionally graded cylindrical shells under combined loads", *Mech. Adv. Mater. Struct.*, **18**(5), 337-346.

Khosravifard, A., Hematiyan, M.R. and Marin, L. (2011), "Nonlinear transient heat conduction analysis of functionally graded materials in the presence of heat sources using an improved meshless radial point interpolation method", *Appl. Math. Modell.*, **35**, 4157-4174.

Moradi-Dastjerdi, R., Foroutan, M. and Pourasghar, A. (2013), "Dynamic analysis of functionally graded nanocomposite cylinders reinforced by carbon nanotube by a mesh-free method", *Mater. Des.*, **44**, 256-266.

Najibi, A. and Shojaeefard, M.H. (2016), "Elastic mechanical stress analysis in a 2D-FGM thick finite length hollow cylinder with newly developed material model", *Acta Mech. Sol. Sinic.*, **29**, 178-191.

Park, K.J. and Kim, Y.W. (2016), "Vibration characteristics of fluid-conveying FGM cylindrical shells resting on Pasternak elastic foundation with an oblique edge", *Thin-Wall. Struct.*, **106**, 407-419.

Rahimi, G.H., Ansari, R. and Hemmatnezhad, M. (2011), "Vibration of functionally graded cylindrical shells with ring support", *Sci. Iranic.*, **18**(6), 1313-1320.

Rezaei Mojdehi, A., Darvizeh, A., Basti, A. and Rajabi, H. (2011), "Three dimensional static and dynamic analysis of thick functionally graded plates by the meshless local Petrov-Galerkin (MLPG) method", *Eng. Analy. Bound. Elem.*, **35**, 1168-1180.

Shakeri, M., Akhlaghi, M. and Hoseini, S.M. (2006), "Vibration and radial wave propagation velocity in functionally graded thick hollow cylinder", *Compos. Struct.*, **76**, 174-181.

Shen, H., Paidoussis, M.P., Wen, J., Yu, D. and Wen, X. (2014), "The beam-mode stability of periodic functionally graded material shells conveying fluid", *J. Sound Vibr.*, **333**, 2735-2749.

Sladek, J., Sladek, V., Stanak, P., Zhang, C. and Wunsche, M. (2013), "Analysis of the bending of circular piezoelectric plates with functionally graded material properties by a MLPG method", *Eng. Struct.*, **47**, 81-89.

Tu, T.M. and Loi, N.V. (2016), "Vibration analysis of rotating functionally graded cylindrical shells with orthogonal stiffeners", *Lat. Am. J. Sol. Struct.*, **13**(15), 2952-2969.

Ugural, A.C. and Fenster, S.K. (2003), *Advanced Strength and Applied Elasticity*, 4th Edition, Prentice Hall.

Wu, C.P. and Liu, Y.C. (2016), "A state space meshless method for the 3D analysis of FGM axisymmetric circular plates", *Steel Compos. Struct.*, **22**, 161-182.

Xiang, S. and Chen, Y. (2014), "meshless local collocation method for natural frequencies and mode shapes of laminated composite shells", *Struct. Eng. Mech.*, **51**, 893-907.

Xiao, J.R., Batra, R.C., Gilhooley, D.F., Gillespie Jr, J.W. and McCarthy, M.A. (2007), "Analysis of thick plates by using a higher-order shear and normal deformable plate theory and MLPG method with radial basis functions", *Comput. Meth. Appl. Mech. Eng.*, **196**, 979-987.

Zhao, X., Liu, G.R., Dai, K.Y., Zhong, Z.H., Li, G.Y. and Han, X. (2008), "Geometric nonlinear analysis of plates and cylindrical shells via a linearly conforming radial point interpolation method", *Comput. Mech.*, **42**, 133-144.

CC